Production of metastable singlet O_2 photosensitized by NO_2

Theodore C. Frankiewicz* and R. Stephen Berry

Department of Chemistry and the James Franck Institute, University of Chicago, Chicago, Illinois 60637

(Received 18 September 1972)

Energy transfer from electronically excited NO_2 to O_2 has been studied. The NO_2* is produced by irradiation with light having $7000<\lambda<4050$ Å. Observations of light emission from $O_2(a\,^1\Delta_g, v'=0)$, $O_2(a\,^1\Delta_g, v'=1)$, and $O_2(b\,^1\Sigma_g^+, v=0)$ have been made, and from these measurements at various pressures, rates have been measured for production of $O_2(a\,^1\Delta_g, v=0)$ and $O_2(b\,^1\Sigma_g^+, v=0)$ by energy transfer from NO_2*, for quenching of $O_2(b\,^1\Sigma_g^+)$ by O_2, NO_2 and wall collisions, and for quenching of $O_2(a\,^1\Delta_g, v=0)$ by NO_2. The efficiency for $^1\Delta_g$ production is 7.5%±2.5%, per collision quenching NO_2*, and for $^1\Sigma_g^+$ production, 0.14%± 0.02%. The $^1\Delta_g$ production efficiency reported here is considerably greater than our preliminary value of 1%. The metastable O_2 generated in an urban atmosphere by energy transfer from NO_2* is 1%–5% as effective as ambient $O(^3P)$ in initiating the oxidation of alkylated aromatic hydrocarbons and 0.1% or less as effective in the case of small, unsubstituted olefins.

INTRODUCTION

The low-lying metastable states of oxygen, $a\,^1\Delta_g$ and $b\,^1\Sigma_g^+$, have attracted considerable attention recently because they provide a potential means of energy storage within a chemical system and because they are considerably more reactive than the ground state $O_2(^3\Sigma_g^-)$.[1,2] $O_2(^1\Delta_g)$, which we will refer to simply as $^1\Delta_g$, at 0.98 eV above the ground state and with a radiative lifetime of 45 min, has received the greatest attention due to recent suggestions that it may possibly play a role in the oxidation of atmospheric hydrocarbons.[3,4] $O_2(^1\Sigma_g^+)$, hence referred to as $^1\Sigma_g^+$, at 1.63 eV above the ground state and with a radiative lifetime of 12 sec, is more reactive than $^1\Delta_g$, but is so rapidly quenched by N_2, O_2, and H_2O [2,5] that it is doubtful this species will be an important atmospheric oxidant.

This work is concerned with determining the efficiency of and the specific states generated by a photosensitized process for generating $^1\Delta$ and $^1\Sigma$ which may be loosely represented by

$$^2NO_2 + h\nu\,(\lambda > 4000\text{ Å}) \xrightarrow{k_1} {}^2NO_2^*, \quad (1)$$

$$^2NO_2^* + {}^3O_2 \rightarrow {}^2NO_2 + {}^1O_2. \quad (2)$$

If metastable $^1O_2$ is to play a detectable role in atmospheric processes, there must be a rather efficient mechanism for its production. Oxygen atoms and hydroxyl radicals, two species present in the normal atmosphere at extremely low concentrations (10^4–10^6 cm^{-3}), are 10^3–10^8 more efficient than $^1O_2$ in initiating hydrocarbon oxidation reactions.[6–10] In the advanced stages of a photochemical smog, ozone is present and will also be an important oxidative species.[6,11] Thus if $^1O_2$ is to contribute to an observable degree to the atmospheric oxidation of even the most susceptible hydrocarbons, its concentration must exceed the O-atom and OH radical concentration by a minimum of 2–3 orders of magnitude. One potential mechanism for generating $^1O_2$ begins with NO_2 absorbing light between 4000 and 7000 Å, without dissociating. The absorption of light with wavelengths less than 4000 Å causes at least partial dissociation of NO_2; for $\lambda<3850$ Å, dissociation occurs with unit quantum efficiency.[12–14] Electronically excited NO_2 is quenched rapidly by many gases. For oxygen, the quenching rate constant is 1.7×10^{-11} cm^3/molecule·sec (corrected from a value based on an NO_2* radiative lifetime of 44 μsec to the newer value of 75 μsec).[15–17] It was not known whether oxygen quenching of NO_2* could result in the electronic excitation of the O_2 molecule. Electronic energy transfer between NO_2* and O_2 is spin allowed and can occur between essentially isoergic states. The reverse energy transfer process represented by

$$^1\Delta_g + {}^1\Sigma_g + NO_2 \rightarrow 2O_2 + NO_2^* \quad (3)$$

has been observed, but was not studied in detail.[18,19]

The purpose of this work was to determine the efficiency of $^1\Delta$ and $^1\Sigma_g^+$ production via (2) and to determine the kinetic paths by which these species are produced and destroyed in this chemical system. We have obtained rate coefficients for the net production of $^1\Delta_g(v'=0)$ under conditions where vibrational relaxation occurs, the production of $^1\Sigma_g(v'=0)$, the quenching rate of $^1\Delta_g$ by NO_2, and the quenching rates of $^1\Sigma_g^+$ by NO_2, O_2, and the cell wall.

Preliminary reports on the production rates $^1\Delta_g$ were published by Jones and Bayes[20] and by ourselves.[21] Our final value for $^1\Delta(v=0)$ production differs considerably from that reported in Ref. 21 because the new results take into account the production of $^1\Delta(v\geq1)$ as well as $^1\Delta(v=0)$ in our system. The Jones and Bayes results of Ref. 20, when integrated over wavelength between 4000 and 7000 Å, agree with ours within about a factor of 2.

EXPERIMENTAL

The apparatus consists of a phosphorimeter with mechanical chopping of the incident excitation light and electronic modulation of the detection system. The latter feature permits time-resolved as well as "steady state" experiments. A xenon arc lamp is used as an ex-

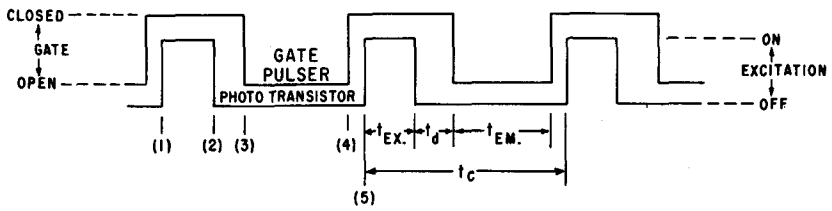

FIG. 1. The operation of the gate pulser and Peatman–Weiner gate. t_{EX} is the time per cycle during which excitation beam is on, t_d is the delay time between end of excitation and start of observation, t_{EM} is the time per cycle during which photoemission is observed, and t_c is the total time per cycle. Sequence of events: (1) excitation beam on, gate closed, (2) excitation beam off, gate pulser triggered, (3) gate pulser voltage drops to 0 and opens gate, (4) gate pulser voltage to +6 closes gate, (5) excitation beam on, starts next cycle.

citation source. The light is focused, filtered with Corning colored glass filters 3–74 and 1–75 to eliminate ultraviolet and infrared, chopped, collimated, and passed through a gas reaction cell containing mixtures of O_2 and NO_2. Light emitted by O_2* in the cell passes through interference filters to isolate 7619 Å, 1.06 μ, or 1.27 μ radiation and strikes a cooled (−78°C) RCA 7102 photomultiplier operated at +1400 V with a dynode string which places the maximum allowable voltage between the photocathode and the first dynode, to minimize statistical fluctuations in the signal.

Single photon pulses from the photomultiplier are fed into an Ortec 260 Time Pick-Off unit which discriminates against low pulse-height noise, amplifies the single photon pulses, and sends an amplified pulse to a fan-out buffer in the Ortec Time Pick-Off Control. Standard logic pulses from the control unit are routed through a gate and used to drive an Eldorado counter.

Gating is controlled by a GE L14B phototransistor which conducts only when illuminated. The signal thus obtained triggers a gate pulser which opens the counting gate for a desired interval after a specified delay during each modulation cycle. A typical modulation cycle is depicted in Fig. 1.

The experiments were performed by taking a series of 10 sec counts first with the cell empty and then with NO_2+O_2 in the cell. The number of 10 sec counts taken for any experiment varied with the intensity of the signal in order to obtain statistical uncertainty in the mean value of a set of counts that was smaller than the average percentage error in other experimental parameters. The expected error of the mean of a number of measurements is $\sigma_{\bar{x}}=\sigma_x/n^{1/2}$ where σ_x is the standard deviation of the individual measurements and n is the total number of measurements. $\sigma_{\bar{x}}$ for the $^1\Delta$ experiments was typically ± 1 count/10 sec and ± 4 counts/10 sec for the $^1\Sigma$ experiments. The number of measurements n was typically 24 for the $^1\Sigma$ experiments and 60 for the $^1\Delta$ experiments. Since "signal" was taken as the difference with and without NO_2+O_1 in the cell, $2\ \sigma_{\bar{x}}$ represents the statistical uncertainty in our intensity measurements.

Not all experiments were conducted in a steady state. However, the phosphorimeter response was analyzed and the results of each experiment were converted to an equivalent steady state intensity for use in determining the energy transfer mechanism. The analysis used was a generalization of that given by O'Haver and Winefordner for a commercial phosphorimeter.[22] The results showed that our instrument yielded a steady-state response if the lifetime of an emitting state exceeded 6 msec. The analysis also showed that, because of the short lifetime of the $^1\Sigma$ species, this response was 12.5% of the true steady-state intensity obtainable with constant observation and excitation. The observed response was 25% of true steady state in the case of $^1\Delta$ experiments, simply because the duty cycle was only 25%.

Since $^1\Sigma$ lifetimes in our experiments were as low as 2.9 msec, recorded $^1\Sigma$ emission intensities were multiplied by a correction factor, $(I/I_{ss})^{-1}$, obtained from the calculated instrument response curve.[23] This curve is similar to that given in Ref. 22.

NO_2 pressures were measured on an Alphatron ionization gauge which has a linear response from 10^{-4} to 10^4 torr for most gases. The gauge reading is calibrated for dry air only. A gauge reading correction factor of 0.54 was determined for NO_2 for pressures below 10 mm where the N_2O_4 degree of dissociation is 85% or higher.[24] The NO_2 used in the experiments was from Matheson and was purified by drying over P_2O_5, oxidizing with 1 atm of O_2 for 24 h,[25,26] and repeated degassing and zone freezing. Pure white N_2O_4 was stored in darkness at −80°C.

The output of the Xe arc lamp between 4000 and 6500 Å (as determined from the manufacturers published spectrum and from absolute intensity measurements at selected wavelengths through narrow band interference filters, with a calibrated Spectra Physics 401B power meter) is shown in Fig. 2 along with the NO_2 absorption spectrum for the same region. From these data, the number of photons absorbed by NO_2 during each modulation cycle may be calculated. Incident light with wavelengths below 4050 Å was blocked to an intensity at most 10^{-5} of that at higher wavelengths (by the 3–74 and 1–75 Corning glass filters) to prevent photodissociation of the NO_2.

The geometry of the region subtended by the detec-

tor was carefully analyzed since we wished to make absolute measurements. The diffusion of excited states, the distribution of $^1\Delta$ and $^1\Sigma$ formed in the cell, and the geometric parameters of the system were included in the analysis.[23]

In order to evaluate absolute emission rates for $^1\Delta$ and $^1\Sigma$, it is essential to determine the observation geometry accurately.

The observed cell volume in our system consists of a central cylindrical region subtended by all points on the photomultiplier face, and a surrounding series of coaxial hollow cone frustrums which see successively less than the full photocathode active area. The cross section of one such hollow cone frustrum is shown darkened in Fig. 3. The volume elements in this section "see" an average of 44% of the photocathode, and contain a value of 13.4 cm³. To evaluate the contribution of this region, we determine a net effective volume (NEV) given by the integral over the small frustrum-shaped volume elements,

$$\text{net effective volume (NEV)} = \int_{\text{cell}} (\text{fraction of photocathode seen})\, dV.$$

In practice, 8–10 divisions are sufficient to yield an accurate value for this integral. The result is used directly to calculate the fraction of emitters in an observed volume when the emitters are uniformly distributed throughout the cell, as the $O_2(^1\Delta_g)$ species are. In this case

$$\text{NEV/Cell vol.} = 83.6\ \text{cm}^3/725\ \text{cm}^3 = 0.115.$$

In the other limiting case, which applies accurately to almost all of our measurements of the $^1\Sigma_g$ state, all emission occurs within the irradiated central excitation cylinder bounded by dashed lines in Fig. 3. In this case, there is an NEV of 10.8 cm³ whereas the emissions are occurring in a total irradiated volume of 72.2 cm³ (the volume of the excitation beam) so 15% of the emissions are in the observed volume.

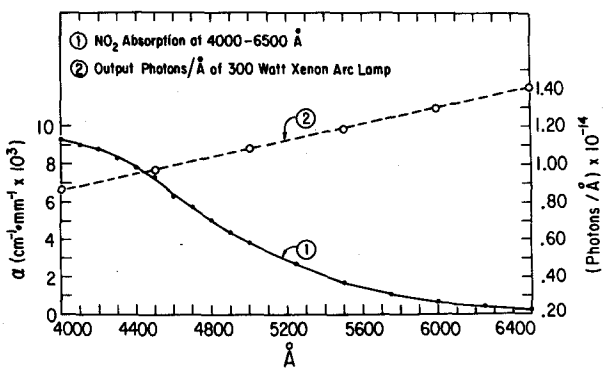

FIG. 2. Wavelength dependence of the absorption coefficient α for NO_2 and the spectral distribution of the 300W xenon arc lamp.

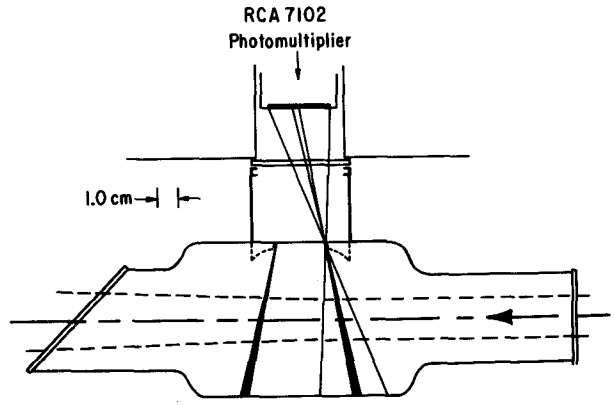

FIG. 3. Geometry of the sample cell with detector and excitation beam, which enters from right. The filter holder separates phototube from cell.

The next consideration is determining the fraction of emissions, originating at a distance R from the photocathode that strike the photocathode. The answer is given approximately as the ratio of the photocathode area seen to the area of the sphere of radius R; or the solid angle $\Omega(R)$ subtended by the small volume dV at the photocathode. The detector records the signal given by the integral of the intensity of emission $I(R)$, multiplied by the fraction of the sphere subtended at R:

$$\text{signal} = \int (4\pi)^{-1}\Omega(R) I(R)\, dV.$$

In our case, $I(R)$ is uniform for the $^1\Delta_g$ state and is determined from the lifetime and diffusion equation for $^1\Sigma_g^+$. The volume is approximately conical so that the volume at distance R increases as R^2, and the solid angle term decreases as $1/R^2$ so the contributions to the observed $^1\Delta_g$ emissions remain very nearly constant as a function of R and equal to that value at the center of the cell. The integrated fraction of the emissions in the total observed volume which strikes the photocathode is 0.006, in both the $^1\Delta_g$ and $^1\Sigma_g^+$ cases.

The RCA 7102 photomultiplier response was determined at all wavelengths of interest. Calibration was against a blackbody source after the method of Stair, Schneider, and Jackson.[27] Results in the near infrared and red differed only slightly from RCA data. No data at 1.27 μ were available. The response across the $O_2[^1\Delta_g(0, 0)]$ emission[28] is shown in Fig. 4. The integrated quantum efficiency of the tube across the band was determined to be 2.3×10^{-7}.

RESULTS AND DISCUSSION

General

We observe the production of both $^1\Delta_g$ and $^1\Sigma_g^+$ in our system as a result of the quenching of photoexcited NO_2 by oxygen. Neither $^1\Delta_g$ nor $^1\Sigma_g^+$ emissions were observed when the illuminated reaction cell contained only O_2, only NO_2, or NO_2+N_2. In addition, by vary-

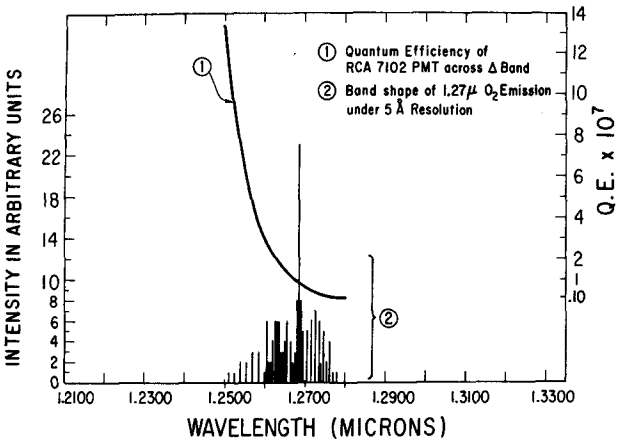

FIG. 4. Wavelength dependence of the quantum efficiency of the RCA 7102 photomultiplier tube and the band shape of the emission band of $O_2(^1\Delta_g)$.

ing the temperature of narrow band interference filters Industrial Optics, 7674 A, 70 Å fwhm; 1.06 μ, 230 Å fwhm; 1.27 μ, 150 Å fwhm) wavelength scans could be made across the $^1\Delta_g$ and $^1\Sigma_g^+$ emission bands. These scans showed no detectable emission away from the expected wavelengths for $^1\Delta$ and $^1\Sigma_g^+$ in our system and establish a mechanism for their production, it is necessary to know the major loss processes and rates for each species. For each state, electronic quenching occurs by collisions with NO_2, O_2, and the cell wall. Energy pooling processes such as

$$^1\Delta + {}^1\Delta \rightarrow {}^1\Sigma + O_2(^3\Sigma_g^-), \quad (4)$$

$$^1\Delta + {}^1\Delta \rightarrow 2\,O_2(^3\Sigma_g^-) + h\nu(6328\text{ Å}), \quad (5)$$

$$^1\Delta + {}^1\Sigma \rightarrow 2\,O_2(^3\Sigma_g^-) + h\nu(4773\text{ Å}), \quad (6)$$

were too slow to affect the low (10^{11}–10^{12} cm^{-3}) singlet oxygen concentrations in our cell.[2] Emission was also considerably slower than gas kinetic quenching rates for $^1\Delta$ and $^1\Sigma$.

Since singlet oxygen is long lived and was formed in the center of our reaction cell, molecular diffusion of the excited states produced $^1\Delta_g$ and $^1\Sigma_g$ concentration gradients across the cell diameter. The diffusion equation was solved for radial diffusion of the excited molecules to ascertain the importance of the cell wall as a quencher. The calculation indicates a uniform $^1\Delta$ concentration in the cell, but $^1\Sigma$ resides mainly near the cell center where it is produced and will be largely quenched before it reaches the cell walls at all but the lowest pressures used (0.9 and 2.0 mm O_2, 0.024 and 0.049 mm NO_2). The problem of using spatially varying concentrations in kinetic equations exists for $^1\Sigma$. To resolve this difficulty, we calculate the total $^1O_2$ production in the cell using the probability that, once formed, a $^1\Delta_g$ or $^1\Sigma_g^+$ molecule will decay by emitting a photon. This emission probability for any excited state is

$$P_E = \text{radiative rate/sum of all loss rates.} \quad (7)$$

The production rate of the excited state is then related to the measured emission intensity by

$$I_{\text{meas}} = (\text{production rate})\,(P_E)\,(F), \quad (8)$$

where F is the apparatus factor which relates the absolute isotropic emission rate in the reaction cell to the detected photon counting rate. The following are the parameters included in the calculation of F, with typical values for each parameter, in particular for the $^1\Delta_g(1, 0)$ radiation at 1.06 μ: $t_{\text{observation}}/t_{\text{cycle}}$, 0.35; fraction of emission in the observed volume, 0.11; the fraction emitted in direction of phototube, 0.006; the fraction transmitted by the filter, 0.40; the fraction recorded by the photomultiplier (quantum efficiency), 1.2×10^{-4}; and the fraction of single photon pulses passed by discriminator, 0.44. The result is an apparatus factor $F=4.9\times10^{-9}$ for the observation of $^1\Delta_g(1, 0)$ emissions.

Figure 5 is an energy level diagram with arrows indicating the major transitions occurring in the NO_2–O_2 photoexcited system. Emission from the various excited states are omitted since the rates are slow compared to quenching. Also, the arrows into the $v=9$ and $v=5$ states of $^1\Delta$ and $^1\Sigma_g^+$, respectively, indicate a transfer into the vibronic manifold only and *not* into a specific vibrational level. The important kinetic equations along with the rate constants used or determined in this work are in Table I. The following paragraphs are devoted to a discussion of the individual constants.

$^1\Delta$ Production

At pressures high enough to achieve full vibrational relaxation of $^1\Delta$, the quenching of electronically excited

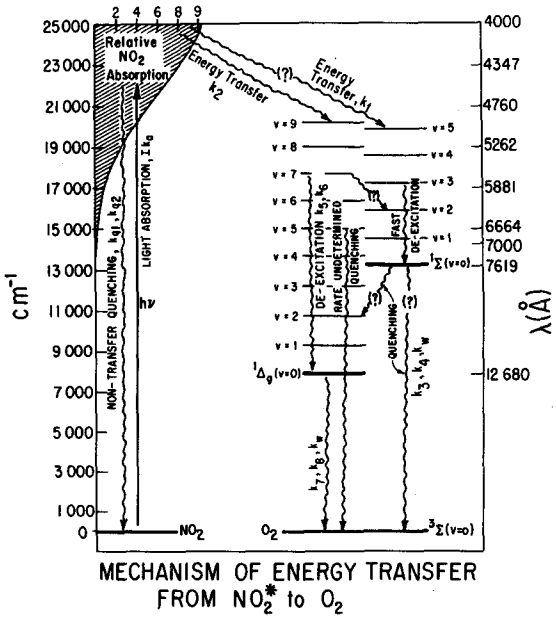

FIG. 5. Mechanism of energy transfer from NO_2^* to O_2. (Question marks indicate processes that were not studied in this work, but that may play a role in the total scheme.)

TABLE I. Kinetic equations for the NO_2^*–O_2 energy transfer (all rate constants in cubic centimeters/molecule·second unless specified).

		Reference
$NO_2+h\nu(\lambda>4000\ \text{Å})\rightarrow NO_2^*$	$I(h\nu)k_0$	26, 39
$NO_2^*+NO_2\rightarrow 2NO_2$	$k_{q1}=4.2\times10^{-11}$ [a]	15, 16
$NO_2^*+O_2\rightarrow NO_2+O_2$	$k_{q2}=2.0\times10^{-11}$ [a]	15
$NO_2^*+O_2\rightarrow NO_2+O_2(^1\Sigma_g^+)$	$k_1=(2.8\pm0.8)\times10^{-14}$	This work
$\rightarrow NO_2+O_2(^1\Delta_g)$ [b]	$k_2=(1.5\pm0.5)\times10^{-12}$	This work
	$k_2\approx0.7\times10^{-12}$	18, 29
$^1\Sigma_g^+ + O_2\rightarrow 2O_2(^1\Delta \text{ or } ^3\Sigma)$	$k_3=(1.4\pm0.2)\times10^{-16}$	This work
$^1\Sigma+NO_2\rightarrow NO_2+O_2(^1\Delta \text{ or } ^3\Sigma)$	$k_4=(1.7\pm0.3)\times10^{-14}$	This work
$^1\Sigma+\text{wall}\rightarrow O_2(^1\Delta \text{ or } ^3\Sigma)$	$\gamma_{\text{wall}}=0.015\pm0.005$ [c]	This work
$^1\Delta(v=0)+O_2\rightarrow 2O_2(^3\Sigma_g^-)$	$k_{11}=2.2\times10^{-18}$	30, 31, 32
$^1\Delta(v=0)+NO_2\rightarrow O_2(^3\Sigma_g^-)+NO_2$	$k_8=(5\pm1)\times10^{-18}$	This work
$^1\Delta(v=0)+\text{wall}\rightarrow O_2(^3\Sigma_g^-)$	$\gamma_{\text{wall}}=1.3\times10^{-5}$ [c]	5, 33

[a] Corrected for an NO_2^* radiative lifetime of ~75 μsec.
[b] For $v'=0$, when $^1\Delta$ undergoes vibrational relaxation; this is about 95% of the total rate for $^1\Delta_g$ production.
[c] γ_{wall} has units of deactivation probability per wall collision.

NO_2 by oxygen results in the production of $^1\Delta(v=0)$ with an efficiency of 7.5%±2.5%. This is about 50 times faster than $^1\Sigma_g^+$ production so it seems likely that $^1\Delta_g$ is formed directly in an $NO_2^*+O_2$ bimolecular collision and not through a $^1\Sigma$ intermediate.

Figure 6 is a summary of the results on the production of $^1\Delta_g(v=0)$ as a function of NO_2 and O_2 pressures as observed by monitoring the $^1\Delta_g(v=0)\rightarrow{}^3\Sigma_g^-(v=0)$ emission at 1.27 μ. In all cases the production of $^1\Delta_g(v=0)$ increased with increasing total gas pressure

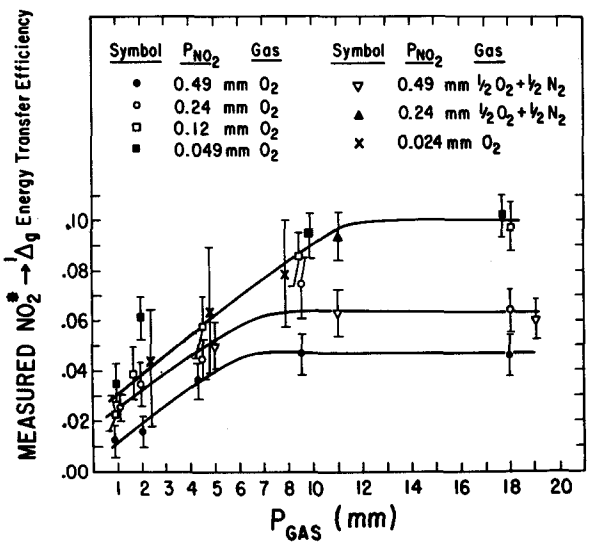

FIG. 6. Observed efficiency of energy transfer from NO_2^* to O_2, to form $^1\Delta_g$, with $v'=0$, as a function of total gas pressure, for various partial pressures of NO_2 in O_2 and in O_2–N_2 mixtures Note that the error bars for the lowest O_2 pressures (—x—) are approximately twice the height of the other error bars, as a result of low signal levels.

until a plateau was reached. The plateau level varied with NO_2 pressure, decreasing if P_{NO_2} was increased above 50 μ but remaining constant below that pressure. The $^1\Delta(v=0)$ production rate constant listed in Table I is for the plateau region where the O_2 pressure is high and the NO_2 pressure is low. In this region there is a low probability of back transfer of energy to NO_2 from vibrationally excited $^1\Delta$, and the $^3\Sigma_g(v=1)$ population is low so it cannot generate a significant $^1\Delta(v=1)$ population (see below).

The change in the measured efficiency of production of $^1\Delta_g(v=0)$, in the low-pressure region (cf. Fig. 6), is probably the result of an O_2–O_2^* collisional relaxation process. We assume that a significant fraction of the $O_2(^1\Delta_g)$ molecules formed by NO_2^*–O_2 collisions appear with at least one quantum of vibrational excitation; this assumption is certainly consistent with the energy diagram of Fig. 5. The simple vibrational relaxation (translation–vibration or rotation–vibration) of O_2 ($^3\Sigma_g^-$) by $O_2(^3\Sigma_g^-)$ is slow.[34] If this were the only radiationless mechanism for deactivating the vibrationally excited $^1\Delta_g$ species also, then we would interpret the falloff in $^1\Delta_g(v=0)$ production at low pressures to inadequate vibrational relaxation of $^1\Delta_g(v\geq1)$.

There are, however, two rapid mechanisms for relaxation of $^1\Delta_g(v=1)$ (and presumably for higher vibrational states) that probably occur; either process gives rise to an apparent production efficiency of $^1\Delta_g(v=0)$ that increases with increasing partial pressure of O_2, at low partial pressures of O_2, and is independent of the partial pressure of O_2 at high pressures. Both mechanisms conform to the description

$$^3\Sigma_g(v=0)+{}^1\Delta_g(v=1)\underset{k_{-9}}{\overset{k_9}{\rightleftharpoons}}{}^3\Sigma_g(v=1)+{}^1\Delta_g(v=0). \quad (9)$$

One process is the near-resonant transfer of a *vibrational*

TABLE II. Typical measured rates for production and relaxation of $^1\Delta_g$.

P_{NO_2} (mm)	P_{O_2} (mm)	I_{meas} (photons/sec)	Measured $^1\Delta(v=0)$ production rate (sec^{-1})	Gas-kinetic collision number, Z_{1-0}, required for $^1\Delta(v=1)$ to give observed $^1\Delta(v=0)$ production
0.049	0.9	0.3	$0.45\times10^{+14}$	0.2×10^{7}
	2.0	1.5	0.81	1.5×10^{7}
	4.5	1.7	1.35	2.0×10^{7}
	17.0	0.3	1.35	1.1×10^{7}
0.12	0.9	1.8	0.74×10^{14}	0.8×10^{7}
	4.5	2.0	1.9	1.8×10^{7}
0.24	0.9	1.5	1.6×10^{14}	0.4×10^{7}
	4.5	1.8	2.9	1.0×10^{7}
0.49	0.9	1.8	1.5×10^{14}	0.5×10^{7}
	4.5	3.5	4.9	1.2×10^{7}
	17.0	1.1	6.0	1.0×10^{7}

quantum, similar to the processes studied by Callear.[35,36] The other process is the transfer of a quantum of *electronic* excitation without transfer of a vibrational quantum. This latter process was recently the object of a study by Jones and Bayes,[37] which demonstrated that electronic energy exchange between $^{32}O_2(^1\Delta_g)$ and $^{36}O_2(^3\Sigma_g^-)$ could occur as often as once in every 10 gas-kinetic collisions.

Applying steady-state conditions to the three species $^1\Delta_g(v=1)$, $^1\Delta_g(v=0)$, and $^3\Sigma_g^-(v=1)$, we readily obtain the dependence of the ratio $^1\Delta_g(v=0)/^1\Delta_g(v=1)$ as follows. We consider only the first excited vibrational state of $O_2(^1\Delta_g)$ for simplicity. The pertinent reactions are (9) and

$$O_2(^3\Sigma_g^-)+NO_2^* \xrightarrow{k_1} {}^1\Delta_g(v=1)+NO_2; \quad (10)$$

$$^1\Delta_g(v=0)+{}^3\Sigma_g{}^1 \xrightarrow{k_{11}} 2\ {}^3\Sigma_g^-, \quad (11)$$

and

$$^3\Sigma(v=1)+{}^3\Sigma_g^-(v=0) \xrightarrow{k_{12}} 2\ {}^3\Sigma_g^-(v=0). \quad (12)$$

The steady-state equations based on these kinetics lead to this equation for concentrations,

$$\frac{[^1\Delta_g(v=0)]}{[^1\Delta_g(v=1)]} = \frac{k_9}{\{k_1 I(\nu) k_{-9} k_{12}/k_{11}^2\}([NO_2]/[O_2]^2)+k_{11}}. \quad (13)$$

We have neglected explicit recognition of the production of vibrationally excited $^3\Sigma_g^-$ by Process (11). However this is unnecessary; the total rate for electronic de-excitation of $^1\Delta_g(v=0)$ is sufficient. The ratio (13) approaches zero as $[O_2]$ or the partial pressure of O_2 goes to zero, and becomes constant at the value k_9/k_{11} as $[O_2]$ grows large. The inference we would like to draw is that the transition from the sloping region to the flat region, in the transfer efficiency curves of Fig. 6, is due to the change from the O_2-dependent to the O_2-independent regions of Eq. (13).

We can test our model by estimating the oxygen pressure at which the two terms in the denominator of (13) become equal. The rate coefficients compiled in Table I and the vibrational relaxation rate for O_2–O_2 collisions[34] give $[O_2]\cong 2\times10^{10}\ [NO_2^*]$ at the equality point, and since $[NO_2^*]\cong(k_{11}/k_{10})[^1\Delta_g]$ and $[^1\Delta_g]\sim10^{11}$–10^{12} cm^{-3}, we obtain $[NO_2^*]\sim10^7$–10^8 and $[O_2, {}^3\Sigma_g^-]\sim0.5$–$5$ torr at the point of equality. The actual turnover from independence of $[O_2]$ to dependence on this variable would appear at slightly higher pressures—as, in fact, the data show in Fig. 5. We therefore consider the interpretation consistent with the data, that rapid exchange and relaxation occur via the process (9).

We measured emission from $^1\Delta_g(v=1)$ to $^3\Sigma_g^-(v=0)$ at 1.06 μ for several NO_2–O_2 pressure combinations. The major loss process for $^1\Delta_g(v=1)$ is quenching by (9) and, secondarily, de-excitation to $^1\Delta_g(v=1)$. The radiative rate for the (1, 0) transition is 5.7×10^{-6} sec^{-1} as calculated from the Franck–Condon factors obtained by Halmann and Laulicht.[38]

Because we can now assume that (9) is rapid, we are justified in equating the rates of production of $^1\Delta_g(v=0)$ and of loss of $^1\Delta_g(v=1)$. This latter, in turn, is very close to the production rate for $^3\Sigma_g^-(v=1)$. These data are summarized in Table II; we see that, again, the interpretation is quantitatively self-consistent.

The rate constant for NO_2 quenching of $^1\Delta_g$ was determined from a Stern–Volmer plot, the equation for $^1\Delta_g(v=0)$ in the reaction cell. The resulting equation is

$$I_0/I=1+\{[k_8/(k_{11}[O_2]+k_f)](1+k''[O_2])\}, \quad (14)$$

where I is the emission intensity in any arbitrary experiment and I_0 is the emission intensity in an experiment where the NO_2 concentration has a very small value, say $[NO_2]_0$, such that NO_2 plays no role in

quenching $^1\Delta_g$. Equation (14) is derived assuming $[NO_2]_0 \ll [NO_2] \ll [O_2]$. k'' is a rate constant related to the net rate at which $^1\Delta_g(v=1)$ is produced; it is not simply k_{10}, because of the possibility that the $v=1$ state is produced via higher v states. Here, we consider k'' to be an empirical constant derived from the oxygen pressure dependence of the $^1\Delta_g(v=0)$ production rate; an experimental value was found, of $k''=3\times10^{-17}$ cm³/molecules·sec. This is again in excellent agreement with the vibrational deactivation rate for $^3\Sigma_g^-(v=1)$. From a plot of (14), the quenching constant k_8 is obtained as $[O_2]$ becomes small. The result is listed in Table I.

Oxygen in its $^1\Sigma_g^+$ state is quenched by NO_2, O_2 and, at low NO_2 pressures, by wall reactions. Wall quenching of $^1\Sigma_g^+$ is partly a diffusion controlled process in our cell; the concentration of $^1\Sigma$ near the wall is a sensitive function of both NO_2 pressure and total gas pressure. The $^1\Sigma_g^+$ is produced only by energy transfer from NO_2* but the exact path is not determined in our experiments since three alternative formation paths are kinetically indistinguishable in our system:

direct formation (I):

$$NO_2^* + O_2 \rightarrow {}^1\Sigma + NO_2, \tag{15}$$

indirect formation (II):

$$\text{(a)}\quad NO_2^* + O_2 \rightarrow {}^1\Delta(v \leqq 3) + NO_2, \tag{16}$$

$$\text{(b)}\quad {}^1\Delta(v \leqq 3) + O_2(v=1) \rightarrow {}^1\Sigma + O_2 \text{ or } NO_2^{\dagger}, \tag{17}$$

indirect formation (III):

$$\text{(a)}\quad NO_2^* + O_2 \rightarrow {}^1\Delta(v \geqq 4) + NO_2, \tag{18}$$

$$\text{(b)}\quad {}^1\Delta(v \geqq 4) + O_2 \rightarrow {}^1\Sigma + O_2 \text{ or } NO_2. \tag{19}$$

We are able to measure only the net overall efficiency for the production of $^1\Sigma$. The results vary from 0.11% to 0.18% as indicated in Figs. 7(a) and 7(b). The corresponding rate constants required to explain the results for each path are

for (I):

$$k_I = (2.8 \pm 0.8) \times 10^{-14} \text{ cm}^3/\text{molecule·sec}, \tag{20}$$

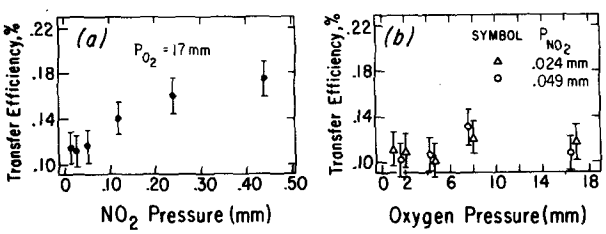

FIG. 7. Energy transfer efficiencies: (a) as a function of NO_2 pressure; (b) as a function of oxygen pressure.

TABLE III. Lifetimes for quenching of $^1\Sigma_g^+$

P_{NO_2} (mm)	P_{O_2} (mm)	τ_{exptl} (msec)	τ_{calc}[a] (msec)
0.049	17.0	8.5	9.6
0.12	4.5	12.3	11.6
	17.0	6.90	6.99
0.24	2.0	6.70	7.05
	4.5	6.40	6.53
	8.5	4.72	5.85
0.49	0.9	2.99	3.65
	2.0	3.51	3.58
	4.5	3.58	3.45
	8.5	3.21	3.25
	17.0	2.85	2.88

[a] Using $k_3=1.4\times10^{-16}$ cm³/molecule·sec and $k_4=1.7\times10^{-14}$ cm³/molecule·sec.

for (IIb):

$$k_{IIb} \sim 10^{-15} \text{ cm}^3/\text{molecule·sec [for } O_2(v=1)], \tag{21}$$

for (IIIb):

$$k_{IIIb} \sim 10^{-15} \text{ cm}^3/\text{molecule·sec (for } O_2). \tag{22}$$

The numbers for (IIb and IIIb) are based on an assumed $^3\Sigma(v=1)/^3\Sigma(v=0)$ ratio near 0.01–0.1 and represent order-of-magnitude estimates only because of uncertainty of this ratio and of uncertainty in the vibrational population of $^1\Delta_g$. As has been discussed, $^1\Delta_g(v\geq1)$ population is significant so either (II) or (III) seems to be a very plausible formation path. This being the case, if NO_2 were about 100 times more effective than O_2 in converting vibrationally excited $^1\Delta_g$ to $^1\Sigma_g^+$, then the effect of NO_2 pressure on the $^1\Sigma_g^+$ production efficiency [see Fig. 6(a)] would be explained.

Lifetime measurements were made on $^1\Sigma$ for 11 NO_2 and O_2 pressure combinations for which wall quenching was expected to be much less important than gas phase quenching as determined by the analysis of diffusion of excited molecules.[23] The lifetime for each combination was determined from the slope of a plot of the log of intensity vs time. In each case, the lifetime is governed by

$$\tau^{-1} = k_3[O_2] + k_4[NO_2], \tag{23}$$

in which k_3 is the rate constant for $^1\Sigma_g^+$ quenching by O_2 and k_4 is the rate constant for $^1\Sigma_g^+$ quenching by NO_2. The constants may be determined from any pair of lifetime curves so it was possible to take several combinations and calculate values. The values for k_3 and k_4 listed in Table I give lifetimes which agree with our experimental measurements to $\pm10\%$ in 9 of 11 cases measured. The data are summarized in Table III.

At high NO_2 pressures the lifetime of $^1\Sigma_g^+$ is suffi-

ciently short to preclude any significant $^1\Sigma_g^+$ concentration near the cell wall even at the lowest oxygen pressure used. In these cases the observed $^1\Sigma_g^+$ production rate was independent of O_2 pressure. However, when both NO_2 and O_2 pressures are low, an apparent decrease in the production rate is observed if wall quenching is neglected. A wall quenching rate for $^1\Sigma_g^+$ of 150 ± 50 sec^{-1}, corresponding to a quenching efficiency $\gamma=0.015\pm0.005$, removes the apparent anomalous effect.

Application to the Atmosphere

There are two major differences between the experimental conditions used to determine the energy transfer mechanism and the atmospheric conditions prevailing in a photochemical smog. The first is the considerably greater background gas pressure which will serve to de-excite rapidly any $^1\Delta_g$ formed by the energy transfer. The second is the lower NO_2 concentrations which result from the higher total gas pressure. Because of these, there will be no possibility for any back transfer of energy to NO_2 and the net energy transfer production of $^1\Delta$ should resemble the plateau region of our experiments with the lower NO_2 pressures used. The fact that our measured transfer rates remained constant as P_{NO_2} was lowered below 50 μ and remained constant as we varied NO_2/O_2 ratios from 600 to 120 000 ppm by varying gas pressure strongly suggests we have indeed measured the rates of elementary molecular processes. These rates may thus be used directly to calculate atmospheric production of $^1\Delta_g$ by the energy transfer from photoexcited NO_2.

Since vibrational de-excitation in the atmosphere is rapid, almost all $^1\Delta$ will be de-excited to $^1\Delta_g(v=0)$. Under this condition, a simplified transfer mechanism is

$$NO_2+h\nu(\lambda>4000\text{ Å})\rightarrow NO_2^*, \tag{24}$$

$$NO_2^*+O_2\rightarrow NO_2+{}^1\Delta_g, \tag{25}$$

$$^1\Delta_g+O_2\rightarrow 2\,O_2. \tag{26}$$

The steady-state kinetic equations for NO_2^* and $^1\Delta_g$ in the atmosphere are

$$d[NO_2^*]/dt=0=k_0I(h\nu)[NO_2]-k_{q2}[NO_2^*][O_2]-k_{q3}[NO_2^*][N_2], \tag{27}$$

$$d[^1\Delta]/dt=0=k_2[NO_2^*][O_2]-k_{11}[^1\Delta][O_2]-k_{q4}[^1\Delta][N_2]. \tag{28}$$

Emission by each species is slow and may be neglected. Since $k_{q4}\ll k_{11}$ while $[O_2]\sim[N_2]$, the last term in (28) may be neglected. $I(h\nu)$ is the photon flux which NO_2 may absorb without dissociating and k_0 is its mean photon absorption rate. The steady-state atmospheric concentration of $^1\Delta$ is

$$[^1\Delta]_{atm}=k_2[NO_2^*][O_2]/k_{11}[O_2]=k_2k_0I(h\nu)[NO_2]/k_{11}k_{q2}[O_2]+k_{q3}[N_2], \tag{29}$$

k_2, k_{11}, k_{q2}, and k_{q3} may be obtained from the literature (see Table I). Inserting these values and values from $[O_2]$ and $[N_2]$ reduces (29) to

$$[^1\Delta]_{atm}=1.5\times10^{-3}k_0I(h\nu)[NO_2]. \tag{30}$$

With values for k_0 from Fig. 2 and values for $I(h\nu)$ given by Leighton,[11] the expression (30) reduces further to

$$[^1\Delta]_{atm}=2.0\times10^6\phi[NO_2\text{ in pphm}], \tag{31}$$

where

$$\phi=(\text{av visible solar flux/cm}^2\cdot\text{sec}\cdot100\text{ Å})\times10^{-15}. \tag{32}$$

At a 40° solar zenith angle, ϕ will be near 5×10^{15} photons/cm$^2\cdot100$ Å$\cdot$sec[11] so an $[NO_2]$ of only 10 pphm will yield a $^1\Delta$ concentration of 10^8/cm^3.

A similar expression may be developed for the atmospheric concentration of $O(^3P)$. The kinetic equations are

$$NO_2+h\nu(\lambda<4000\text{ Å})\rightarrow NO+O(^3P) \tag{33}$$

and

$$O+O_2+M\rightarrow O_3+M. \tag{34}$$

The steady-state kinetic equation may be written for $O(^3P)$,

$$[O]=k_0'I'(h\nu)[NO_2]/k_{O_3}[O_2][M], \tag{35}$$

where $k_0'I'(h\nu)$ is the rate of dissociative photon absorption by NO_2 and k_{O_3} is the third-order rate constant for ozone formation. Johnston[6] has determined $k_{O_3}=6.4\times10^{-34}$ (cm^3)^2/molecule$\cdot$sec.

Placing this and values for $I(h\nu)$ from Leighton, k_0' from Dixon,[39] and for $[O_2]$ and $[M]$ into (31) we obtain

$$[O]=1.13\times10^4\phi'[NO_2\text{ in pphm}], \tag{36}$$

where

$$\phi'=(\text{solar flux per 100 Å at 3300 Å})\times10^{-15}; \tag{37}$$

Again at a 40° solar zenith angle, a ϕ' of 1.45×10^{15} photons/100 Å$\cdot$cm$^2\cdot$sec near 3300 Å is representative.[11] Thus the ratio

$$\frac{[^1\Delta]}{[O]}=\frac{2.0\times10^6\,\phi[NO_2\text{ in pphm}]}{1.13\times10^4\,\phi[NO_2\text{ in pphm}]}=1.77\times10^2\frac{\phi}{\phi'} \tag{38}$$

has the value

$$[^1\Delta]/[O]=6.1\times10^2. \tag{39}$$

Data obtained by Herron and Huie[8,40] and by Ackerman *et al.*[41] indicate that the ratios of reaction rate constants, $k(O^3P)/k(^1\Delta_g)$, for attack on hydrocarbons, vary from greater than 10^6 for small olefins found in the atmosphere, to 7×10^4 for σ-xylene which is also found in the atmosphere.[42] From these data, it can be seen that $^1\Delta$ generated by energy transfer from NO_2^* will initiate a small fraction of the oxidation of hydrocarbons and the ratio of this initiation to that by $O(^3P)$ will be 0.01–0.05 for alkylated aromatics and 0.001 or less for small, unsubstituted olefins.

CONCLUSIONS

We conclude that there is at least one mechanism for generating a steady-state atmospheric concentration of $^1\Delta$ in excess of $10^8/cm^3$ and that only a small contribution to the smog oxidation reactions will be made by this species.

We conclude further that the transfer of electronic energy from NO_2* to O_2 generates $^1\Delta_g$ in a vibrationally excited state which is possibly an intermediate for $^1\Sigma_g^+$ formation in this system. The net efficiency of $^1\Delta_g$ production is $7.5\%\pm2.5\%$ and that for $^1\Sigma_g^+$ is $0.14\%\pm0.02\%$. Vibrationally excited $^1\Delta_g$ also appears to transfer energy rapidly back to NO_2.

Whether a concentration of order 10^8 cm^{-3} for $^1\Delta_g$ makes this species a significant factor for oxidation of species other than hydrocarbons is not known, nor is it known whether this concentration is high enough to be of ambient biological importance.

ACKNOWLEDGMENTS

We would like to acknowledge the financial support of the Petroleum Research Foundation and of the National Science Foundation for the support of this research. We would also like to acknowledge helpful conversations with Dr. K. D. Bayes, especially for pointing out the rapid energy exchange processes for vibrationally excited $^1\Delta_g$ oxygen molecules.

* Petroleum Research Foundation Fellow; present address: Chemistry Division Naval Research Laboratory, Washington, D.C. 20390.

[1] D. R. Kearns, Chem. Revs. **71,** 395 (1971).
[2] R. P. Wayne, Adv. Photochem. **7,** 311 (1969).
[3] J. N. Pitts, A. U. Khan, and E. B. Smith, Environ. Sci. and Technol. **1,** 656 (1967).
[4] R. H. Kummler and M. H. Bortner, J. of Geophysical Res. **75,** 3115 (1970).
[5] K. H. Becker, W. Groth, and V. Schurath, Chem. Phys. Lett. **8,** 259 (1971).
[6] H. S. Johnston, J. N. Pitts, J. Lewis, L. Zafonte, and T. Mattershead, Univ. of California Project Clean Air Task Force Rept. No. 7, 1971.
[7] B. Weinstock and H. Niki, Science **176,** 290 (1972).
[8] R. E. Huie and J. T. Herron, Int. J. Chemical Kinetics (to be published).
[9] J. C. McConnell, M. B. McElroy, and S. C. Wofsy, Nature **233,** 187 (1971).
[10] E. D. Morris, Jr., D. H. Stedman, and H. Niki, J. Am. Chem. Soc. **93,** 3570 (1971).
[11] P. A. Leighton, *Photochemistry of Air Pollution* (Academic, New York, 1961).
[12] A. E. Douglas and K. P. Huber, Can. J. Phys. **43,** 7481 (1965).
[13] (a) R. J. Cvetanovic, J. Air Poll. Contr. Assoc. **14,** 208 (1964). (b) E. A. Schuck, E. R. Stephens, and R. R. Schrock, J. Air Poll. Contr. Assoc. **11,** 695 (1966).
[14] I. T. N. Jones and K. D. Bayes, "The Photolysis of Nitrogen Dioxide" (unpublished); photodissociation seems to be complete for $\lambda<3980$ Å.
[15] G. H. Meyers, D. M. Silver, and F. Kaufmann, J. Chem. Phys. **44,** 718 (1966).
[16] S. E. Schwartz and H. Johnston, J. Chem. Phys. **51,** 1286 (1969).
[17] P. B. Sackett and J. T. Yardley, Chem. Phys. Lett. **6,** 323 (1970).
[18] R. A. Young and G. Black, J. Chem. Phys. **47,** 2311 (1967).
[19] S. J. Arnold, M. Kuba, and E. A. Ogryzlo, Adv. Chem. Ser. **77,** 133 (1968).
[20] I. T. N. Jones and K. D. Bayes, Chem. Phys. Lett. **11,** 163 (1971).
[21] T. C. Frankiewicz and R. S. Berry, Environ. Sci. and Technol. **6,** 365 (1972).
[22] T. C. O'Haver and J. D. Winefordner, Analytical Chem. **38,** 602 (1966).
[23] T. C. Frankiewicz, Ph.D. thesis, University of Chicago, 1972.
[24] H. Blend, J. Chem. Phys. **53,** 4497 (1970).
[25] D. Neuberger and A. B. F. Duncan, J. Chem. Phys. **22,** 1693 (1954).
[26] T. C. Hall and F. E. Blacet, J. Chem. Phys. **20,** 1745 (1952).
[27] R. Stair, W. E. Schneider and J. K. Jackson, Appl. Op. **2,** 1152 (1963).
[28] L. Herzberg and G. Herzberg, Astrophys. J. **105,** 353 (1947).
[29] I. T. N. Jones and K. D. Bayes (private communication).
[30] F. D. Findlay, C. J. Fortin, and D. R. Snelling, Chem. Phys. Letters. **3,** 204 (1969).
[31] I. D. Clark and R. P. Wayne, Chem. Phys. Lett. **3,** 93 (1969).
[32] R. P. Steer, R. A. Ackerman, and J. N. Pitts, Jr., J. Chem. Phys. **51,** 843 (1969).
[33] K. H. Becker, W. Groth, and U. Schurath Chem. Phys. Lett. **8,** 259 (1971); these authors give a value of 1.8×10^{-18} for k_{11}.
[34] B. Stevens, "Collisional Activation in Gases," in *International Encyclopedia of Physical Chemistry and Chemical Physics* (Pergamon, New York, 1967).
[35] A. B. Callear, Discussions Faraday Soc. **33,** 28 (1962).
[36] A. B. Callear and I. W. M. Smith, Trans. Faraday Soc. **59,** 1735 (1963).
[37] I. T. N. Jones and K. D. Bayes, J. Chem. Phys. **57,** 1003 (1972).
[38] M. Halmann and I. Laulicht, J. Chem. Phys. **43,** 438 (1965).
[39] J. K. Dixon, J. Chem. Phys. **8,** 157 (1940).
[40] J. T. Herron and R. E. Huie, Annals N.Y. Acad. Sci. **171,** 229 (1970).
[41] R. A. Ackerman, J. N. Pitts, and R. P. Steer, J. Chem. Phys. **52,** 1603 (1970).
[42] A. P. Altshuller, W. A. Lonneman, F. D. Sutterfield, and S. L. Kopczynski, Environ. Sci. Technol. **5,** 1009 (1971).